iScience

CellPress
OPEN ACCESS

Article

In situ modeling of acquired resistance to RTK/RAS-pathway-targeted therapies

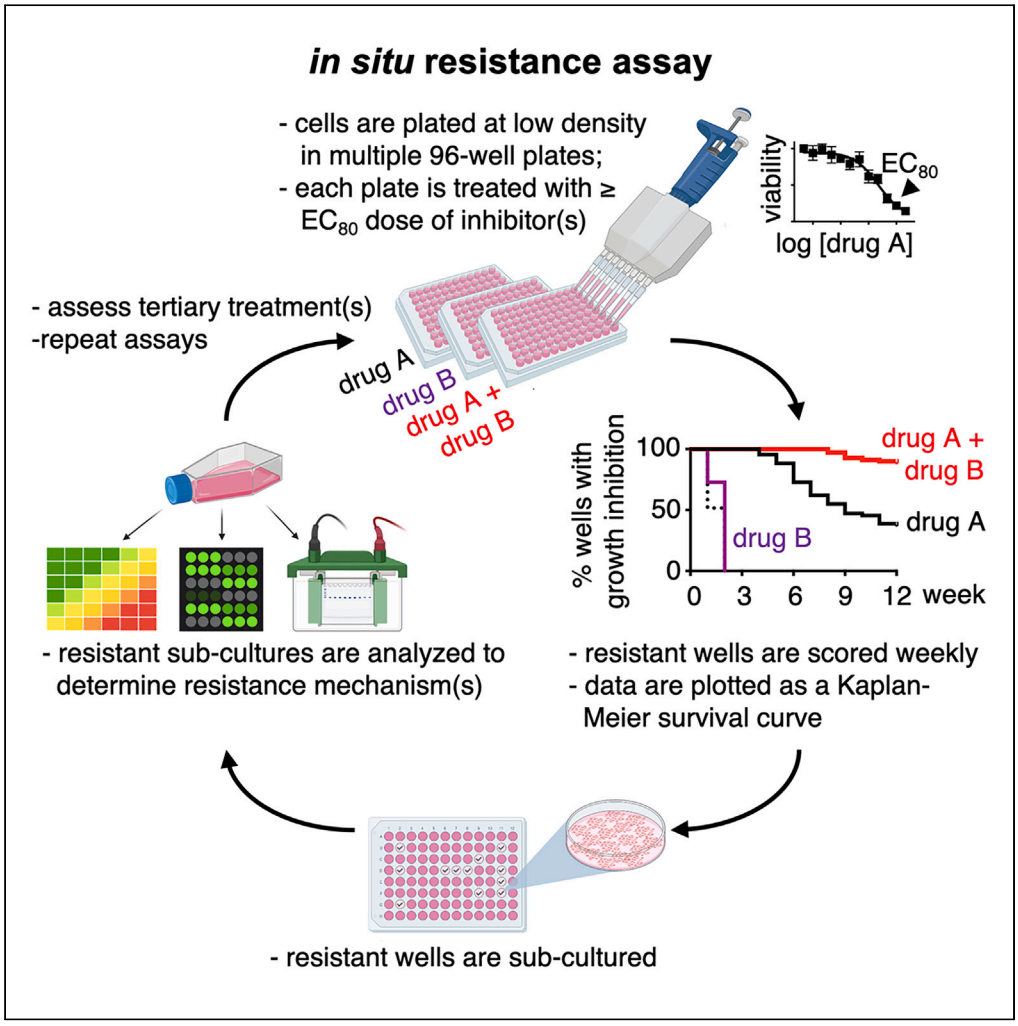

Nancy E. Sealover, Patricia T. Theard, Jacob M. Hughes, Amanda J. Linke, Brianna R. Daley, Robert L. Kortum

robert.kortum@usuhs.edu

Highlights

Acquired resistance to RTK/RAS pathway members can be modeled *in situ*

SHP2 inhibitors reduce the development of acquired osimertinib resistance

Isolated osimertinib-resistant populations show hyperactivation of multiple RTKs

SHP2 inhibitors resensitize resistant populations to osimertinib treatment

Sealover et al., iScience *27*, 108711
January 19, 2024
https://doi.org/10.1016/j.isci.2023.108711

iScience

CellPress
OPEN ACCESS

Article

In situ modeling of acquired resistance to RTK/RAS-pathway-targeted therapies

Nancy E. Sealover,[1,2] Patricia T. Theard,[1,2] Jacob M. Hughes,[1] Amanda J. Linke,[1] Brianna R. Daley,[1] and Robert L. Kortum[1,3,*]

SUMMARY

Intrinsic and acquired resistance limit the window of effectiveness for oncogene-targeted cancer therapies. Here, we describe an *in situ* resistance assay (ISRA) that reliably models acquired resistance to RTK/RAS-pathway-targeted therapies across cell lines. Using osimertinib resistance in *EGFR*-mutated lung adenocarcinoma (LUAD) as a model system, we show that acquired osimertinib resistance can be significantly delayed by inhibition of proximal RTK signaling using SHP2 inhibitors. Isolated osimertinib-resistant populations required SHP2 inhibition to resensitize cells to osimertinib and reduce MAPK signaling to block the effects of enhanced activation of multiple parallel RTKs. We additionally modeled resistance to targeted therapies including the $KRAS^{G12C}$ inhibitors adagrasib and sotorasib, the MEK inhibitor trametinib, and the farnesyl transferase inhibitor tipifarnib. These studies highlight the tractability of *in situ* resistance assays to model acquired resistance to targeted therapies and provide a framework for assessing the extent to which synergistic drug combinations can target acquired drug resistance.

INTRODUCTION

Lung cancer is the leading cause of cancer-related death worldwide; adenocarcinomas are the most common subtype of lung cancer.[1] Oncogenic driver mutations in the RTK/RAS/RAF pathway occur in 75%–90% of lung adenocarcinomas (LUAD). With enhanced understanding of the oncogenic driver mutations causing disease, oncogene-targeted therapies have substantially improved patient outcomes not only for patients with LUAD but across the spectrum of cancer types. However, in most cases resistance to targeted therapeutics develops, necessitating approaches that can either delay therapeutic resistance or treat resistant cancers.

Activating mutations in the epidermal growth factor receptor (EGFR) drive oncogenesis in 15%–30% of LUADs.[1] For patients with *EGFR*-mutated tumors, the EGFR-TKI osimertinib markedly enhances progression-free and overall survival compared with standard chemotherapy[2,3]; however, both intrinsic and acquired osimertinib resistance limit patient survival. Acquired osimertinib resistance is most often driven by RTK/RAS pathway reactivation,[4] either via secondary EGFR mutations or via enhanced signaling through multiple parallel RTKs including MET, AXL, FGFR, HER2/3, and IGF1-R.[4–13] This heterogeneity of RTKs that can drive osimertinib resistance, along with the finding that at rapid autopsy patient tumors often harbor multiple modes of RTK-dependent osimertinib resistance,[14] may limit the up-front effectiveness of combining osimertinib with a second RTK inhibitor.

Upregulation of heterogeneous RTK activity has been documented as an intrinsic and acquired mechanism of resistance in response to mono-therapeutics designed to target RTK-/RAS-driven cancers. The non-receptor protein tyrosine phosphatase SHP2 has been suggested to support RTK activity in drug-resistant cell populations as a ubiquitous regulator of proximal RTK signaling. SHP2 complexes with GAB1 at the plasma membrane in response to growth factor stimulation, consequently recruiting GRB2-SOS complexes from the cytosol to the membrane to transduce signals from activated RTKs signaling to the RAS-MAPK pathway.[15–17] Although combining SHP2 inhibition with an RTK or RAS inhibitor has been shown to be effective, use of SHP2 inhibitors to block intrinsic or acquired resistance is lacking in models with directly measured heterogeneous RTK upregulation. Further, many of these publications do not assess the effect of SHP2 inhibition on a broad timescale representative of acquired resistance. We therefore aimed to develop a model to study the role of SHP2 inhibition in cells that had developed resistance to RTK-targeted therapies over 6–12 weeks and capture the effect of SHP2 inhibition in cells that have heterogeneous RTK upregulation as a response to previous oncogene inhibition.

Historically, combination therapies have been based on identifying two or more active single agents with distinct mechanisms of action,[18] and most current combination therapies include an oncogene-targeted therapy and a second drug that targets an independent mechanism that, if left untargeted, causes to resistance to the first agent.[19,20] Although many of these approaches succeed in increasing windows of progression-free survival (PFS) in patients, resistance still emerges, often due to the strikingly heterogeneous mechanisms of acquired drug

[1]Department of Pharmacology and Molecular Therapeutics, Uniformed Services University of the Health Sciences, Bethesda, MD, USA
[2]These authors contributed equally
[3]Lead contact
*Correspondence: robert.kortum@usuhs.edu
https://doi.org/10.1016/j.isci.2023.108711

resistance both intratumorally[14,21] and across patients.[22,23] Thus, approaches are needed to identify combination therapies that not only address a single mechanism of acquired resistance but simultaneously prevent most common mechanisms of resistance to a given targeted therapy. This need has led to a shift toward groups attempting to identify synergistic drug combinations to treat cancers with specific genetic profiles.[18]

Preclinical studies designed to identify synergistic drug combinations are excellent at capturing the success of a drug treatment within a time frame of 1–14 days. Unfortunately, few studies extend beyond assessing this initial window of efficacy to determine whether combinations can prevent the development of acquired resistance. For example, RNAi and CRISPR screens have been widely successful in identifying often unexpected partners for combination therapies[24–26]; however, the time frame of these approaches biases them toward identifying and assessing secondary drug targets that will limit intrinsic, but not acquired, resistance. Further, those studies that do assess acquired resistance *in situ* are limited to the assessment of a few cell lines established by dose escalation over multiple months (reviewed in[27]) (e.g.,[28–32]) rather than determining the extent to which inhibiting a secondary drug target can delay the onset of resistance. Therefore, a framework of pre-clinical experiments to assess initial efficacy combined with extended *in vitro* approaches such as 6- to 16-week proliferation outgrowth assays[33,34] and time-to-progression (TTP) assays[26] can provide robust evidence for proposing effective and rational combination therapies that is accessible and scalable.

Here, we describe an *in situ* resistance assay (ISRA) that allows us to (1) assess the development of acquired resistance in a large cohort of individual cultures, (2) isolate multiple therapy-resistant polyclonal cell populations for biochemical analysis, and (3) test the effectiveness of combination therapies to delay the development of acquired resistance. We used *EGFR*-mutated LUAD cell lines as a model to assess the time frame of acquired resistance to the third-generation tyrosine kinase inhibitor (TKI) osimertinib in an *in situ* resistance assay (ISRA) that combines elements from proliferation outgrowth[34] and TTP[26] assays and allows for screening of drug combinations in large numbers of individual cell populations using a 96-well format. We show that cells isolated from osimertinib ISRAs remain osimertinib resistant and have developed acquired resistance via upregulation of multiple parallel RTKs. Using a panel of inhibitors targeting multiple receptor tyrosine kinases (RTKs) and RTK-associated proteins, we found that inhibiting proximal RTK signaling using the SHP2 inhibitor RMC-4550[35] most consistently increased both efficacy and potency of osimertinib across all osimertinib-resistant cell lines. In addition to re-sensitizing osimertinib-resistant lines to osimertinib, we further showed that SHP2 inhibition both delayed the onset and reduced the overall frequency of osimertinib-resistant cultures. This model supports the suggested mechanism that SHP2 acts a central signaling node for RTK upregulation during acquired drug resistance. Finally, we demonstrated the broad applicability of ISRAs to model acquired resistance to multiple targeted including the $KRAS^{G12C}$ inhibitors adagrasib and sotorasib, the MEK inhibitor trametinib, and the farnesyl transferase inhibitor tipifarnib in multiple cell line models.

RESULTS

Development of an assay to model acquired resistance *in situ*

We sought to develop an *in situ* resistance assay (ISRA) that modeled the development of acquired resistance to targeted therapies and could be performed in a multi-well setup to mimic a multiple-subject trial testing the effectiveness of drug combinations to limit the development of resistance. To develop and optimize the ISRA, we used a panel of *EGFR*-mutated lung adenocarcinoma (LUAD) lines treated with the third-generation TKI osimertinib, as the mechanisms driving osimertinib resistance in LUAD are well established.[4–13] To establish the doses of osimertinib that inhibits survival ($\geq EC_{50}$) in the panel of *EGFR*-mutated cell lines, H1975 (L858R/T790M), H827 (exon 19 deletion), PC9 (exon 19 deletion), and PC9-TM (exon 19 deletion with an acquired T790M mutation[36]) cells were treated with increasing doses of osimertinib, and cell viability was assessed four days after treatment (Figures 1A and 1B). The doses of osimertinib that inhibited survival were similar across all *EGFR*-mutated cell lines [EC_{50} (17–46 nM)–EC_{85} (200–450 nM)], allowing us to use similar doses in each cell line to determine the concentration of osimertinib that caused prolonged growth arrest (>6 weeks) prior to cell outgrowth in a majority of cell populations for each cell line. Cells were plated at low density (250 cells/well; <10% confluent) in multiple 96-well plates, and each plate was either left untreated (to assess the time required for normal cell outgrowth) or treated with a single inhibitory dose of osimertinib (EC_{50}–EC_{85} range; 30, 50, 150, or 300 nM) for up to 12 weeks. Cells were fed weekly with fresh media and inhibitor. The inner 60 wells of each plate were visually assessed weekly, and wells that were ≥50% confluent were scored as resistant to that dose of osimertinib. Visual assessment of confluence can be subjective, thus, there is the opportunity for "bias" of assessing whether well among different conditions achieve >50% confluence on a given week. However, we routinely observed that (1) once cultures started expanding beyond isolated (single or 2–3) cells, they expanded to 50% confluence in 2–4 weeks and (2) wells scored at 50% confluence achieved 80%–90% confluence one week later. Thus, we estimate that the accuracy of assessing each well as resistant is $\pm$1 week.

Lower doses of osimertinib corresponding to the EC_{50}-EC_{75} caused a 1- to 3-week delay in the outgrowth of cells, whereas cells treated with $\geq EC_{80}$ of osimertinib showed prolonged growth arrest before regaining proliferative capacity (Figure 1C) under continuous osimertinib treatment, indicative of cells that had become osimertinib resistant. These results suggest that osimertinib resistance can be modeled *in situ* using doses of osimertinib with $\geq EC_{80}$ for growth inhibition in *EGFR*-mutated LUAD cell lines.

Acquired osimertinib resistance is commonly driven by RTK/RAS pathway reactivation[4] either via secondary EGFR mutations or enhanced signaling through one or more parallel RTKs including MET, AXL, FGFR, HER2/3, and IGF1-R. Given the multiplicity of RTKs capable of driving osimertinib resistance, we posited that inhibition of proximal RTK signaling, via SHP2 inhibition, would limit RTK-dependent osimertinib resistance and thereby prolong the initial window of osimertinib therapy. To directly assess the extent to which SHP2 inhibition could limit the development of acquired osimertinib resistance, we performed ISRAs in *EGFR*-mutated H1975 and PC9 cells treated with osimertinib either

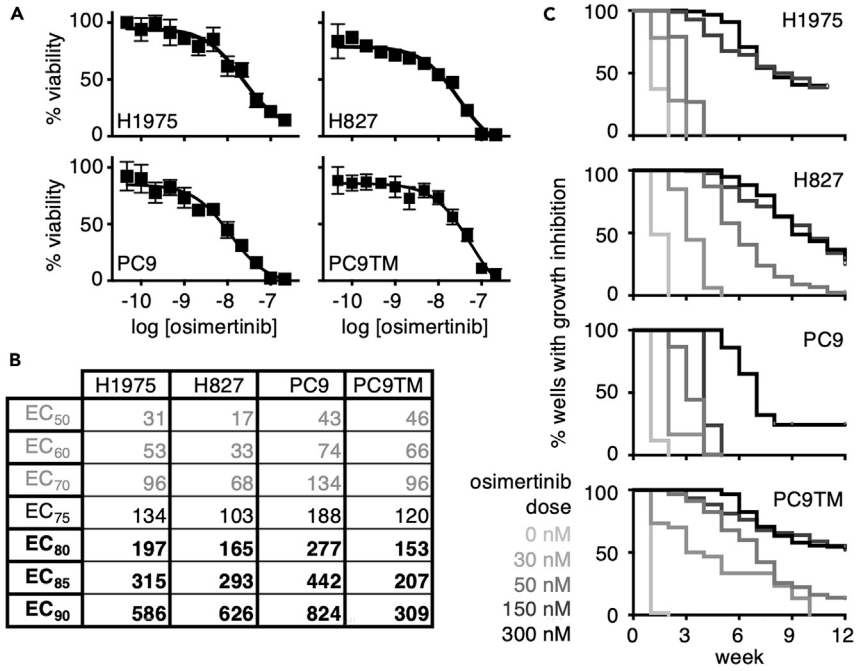

	H1975	H827	PC9	PC9TM
EC_{50}	31	17	43	46
EC_{60}	53	33	74	66
EC_{70}	96	68	134	96
EC_{75}	134	103	188	120
EC_{80}	**197**	**165**	**277**	**153**
EC_{85}	**315**	**293**	**442**	**207**
EC_{90}	**586**	**626**	**824**	**309**

Figure 1. Modeling osimertinib resistance *in situ*

(A and B) Dose-response curves (A) and EC_{50}–EC_{90} values (B) for the indicated *EGFR*-mutated LUAD cell lines treated with osimertinib under anchorage-dependent conditions. Data in (A) are mean ± SD from n = 3 independent experiments.

(C) EGFR-mutated cell lines were plated at low density (250 cells/well) in replicate 96-well plates, and each plate was treated with the indicated dose of osimertinib. Wells were fed and assessed weekly for outgrowth; wells that were >50% confluent were scored as resistant to the given dose of osimertinib. Data are plotted as a Kaplan-Meyer survival curve. Plates treated with ≥ the EC_{80} osimertinib dose [see bold values in (B)] showed an extended inhibition of growth followed by outgrowth of individual colonies consistent with true drug resistance. Data in (C) are combined from n = 3 independent trials.

alone or in combination with two distinct SHP2 inhibitors [RMC-4550 or SHP099 (Figure 2)]. When treated with osimertinib alone at either 150 or 300 nM, H1975 cells show a median time to outgrowth of 9 weeks with 63% of populations eventually becoming osimertinib resistant. Combining RMC-4550 or SHP099 with osimertinib significantly inhibited the development of osimertinib resistance, with only 3% (RMC-4550) or 21% (SHP099) of populations treated with combination therapy showing outgrowth at 12 weeks.

Similar results were observed in PC9 cells treated with 300 nM osimertinib. Cells treated with osimertinib alone showed median time to outgrowth of 8 weeks with 76% of total populations becoming osimertinib resistant. Combining RMC-4550 or SHP099 with 300 nM osimertinib significantly inhibited the development of osimertinib resistance, with only 30% (RMC-4550) or 41% (SHP099) of populations treated with combination therapy showing outgrowth at 12 weeks. Further, although PC9 cells treated with 150 nM osimertinib show rapid outgrowth (median time to outgrowth of 4 weeks), this outgrowth was significantly delayed by either RMC-4550 or SHP099. Overall, these data show both the utility of ISRAs to test the extent to which therapeutic combinations can inhibit the development of acquired resistance and show that SHP2 inhibition may significantly prolong the window for osimertinib therapy.

RTK phosphorylation is heterogeneously upregulated in osimertinib-resistant cells

We next wanted to assess if the mechanisms driving acquired osimertinib resistance in cells isolated from IRSAs would be predictive of sensitivity to SHP2 inhibition. We isolated and expanded a cohort of osimertinib-resistant populations (OR1-8) from H1975 individual wells treated with 150 nM osimertinib to investigate the extent to which (1) individual populations maintained osimertinib resistance and (2) the mechanisms driving osimertinib resistance in cells isolated from continued drug treatment were similar to those seen in patient populations and predictive of sensitivity to proximal RTK pathway inhibition using a SHP2 inhibitor. Dose-response studies showed that osimertinib was much less potent in all eight OR populations compared with H1975 parental cells (Figures 3A and S1A), with >40% of cells surviving when treated with 1000 nM osimertinib compared with <20% of parental controls. Further, in ISRA assays using 150 nM osimertinib, all eight populations showed osimertinib resistance (Figures 3B and S1B). While it took 9 weeks for 50% of parental H1975 wells to become osimertinib resistant and only 70% became resistant in the 12-week assay, OR1-8 populations showed outgrowth in 100% of wells within 3–5 weeks (Figures 3B and S1B). These data confirm that cell populations isolated from ISRAs maintain drug resistance.

Osimertinib resistance is most often driven by RTK/RAS pathway reactivation via either tertiary EGFR mutations or enhanced signaling through parallel RTKs including MET, AXL, HER2/3, and FGFR.[5–13] To assess for tertiary EGFR mutations, we sequenced the *EGFR* kinase

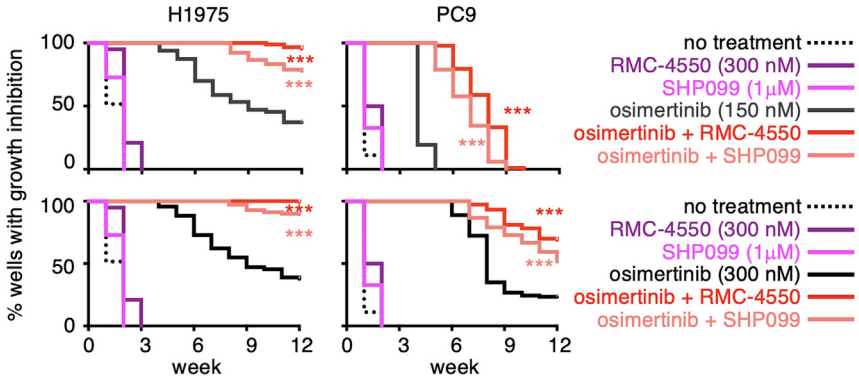

Figure 2. SHP2 inhibition limits the development of osimertinib resistance

EGFR-mutated H1975 and PC9 cells were plated at low density (250 cells/well) in replicate 96-well plates, and each plate was either left untreated (black, dashed) or treated with osimertinib alone at 150 nM (dark gray) or 300 nM (black), a SHP2 inhibitor alone (RMC-4550 at 300 nM or SHP099 at 1 mM) (purple), or the combination of osimertinib + RMC-4550 or SHP099 (red). Wells were fed and assessed weekly for outgrowth; wells that were >50% confluent were scored as resistant to the given dose of osimertinib. Data are plotted as a Kaplan-Meyer survival curve. ***p < 0.001 vs. osimertinib drug treatment. Data are combined from n = 3 independent trials.

domain for each osimertinib-resistant population. Osimertinib-resistant H1975 populations did not show tertiary EGFR mutations (data not shown), suggesting that non-EGFR-dependent mechanisms drive osimertinib resistance in H1975 cells. To assess whether, similar to patient samples, OR populations isolated from ISRAs showed hyperactivation of parallel RTKs, we evaluated OR1-8 populations for changes in magnitude of receptor tyrosine phosphorylation compared with parental H1975 cells using phosphotyrosine arrays (Figures S2 and S3A). Only two of eight osimertinib-resistant populations showed increased EGFR phosphorylation (Figures S3A and S3B), suggesting non-EGFR-dependent mechanisms were responsible for the majority of osimertinib resistance. Indeed, OR1-8 populations showed increased phosphorylation of multiple RTKs; AXL and FGFR2-α most consistently showed increased phosphorylated across OR1-8 populations compared with parental H1975 cells (Figure 4A), with additional RTKs including c-MET, RET, IGF-1R, c-KIT, and TIE2 and non-receptor kinases ABL and SRC family kinases (SFKs), showing increased phosphorylation in at least two OR populations (Figures 4A and S3A–S3D). These data show that osimertinib-resistant populations isolated from ISRAs show reactivation of multiple RTKs, distinct from EGFR, similar to the multiple mechanisms of RTK reactivation observed in osimertinib-resistant tumors from rapid autopsy studies.[14]

SHP2 inhibition resensitizes osimertinib-resistant cells to osimertinib regardless of specific receptor activity

The current treatment paradigm for patients with osimertinib-resistant tumors is to determine secondary therapy based on the presence of druggable mechanism(s) of osimertinib resistance, most often using inhibitors of mutated or amplified RTKs. To determine the extent to which treatment with inhibitors of RTKs or non-receptor kinases showing hyperactivation in osimertinib-resistant cells resensitized these cells to osimertinib, we used a panel of RTK inhibitors and the ABL/SFK inhibitor dasatinib; primary and secondary targets of each inhibitor are shown in Figure S3E. We treated OR1-8 populations with either increasing doses of each secondary inhibitor from Figure S3E ± 10 nM osimertinib (Figure S4, top) or increasing doses of osimertinib ±100 or 300 nM the second inhibitor (Figure S4, bottom). Synergistic drug-drug interactions were assessed by Multi-dimensional Synergy of Combinations (MuSyC) to deconvolute synergistic potency [Log(α_2)] and efficacy (β_{obs})[37,38]; optimal drug combinations show positive values for both Log(α_2) and β_{obs} and fall in the upper right quadrant of plots for these two indices of synergy. Although individual combinations showed modest increases in synergistic potency and efficacy in specific cell lines (crizotinib and cabozantinib in OR1; linsitinib in OR1 and OR2; SGI-7079 in OR8), overall, the effect of specific RTK inhibitors or dasatinib was heterogeneous among OR cell lines and not correlated with increased RTK signaling of the major target of any of the inhibitors tested (Figures 4B–4D). In contrast, while inhibition of proximal RTK signaling using the SHP2 inhibitor RMC-4550 did not significantly inhibit survival of OR1-8 populations alone (Figure S4), RMC-4550 increased the potency [Log(α_2)] and efficacy (β_{obs}) of osimertinib in all OR1-8 populations (Figures 4E–4G). To further characterize the extent to which RMC-4550 synergized with osimertinib in osimertinib-resistant populations, we treated parental H1975 or OR1-8 with increasing doses of RMC-4550 and/or osimertinib in a 6x10 matrix of drug combinations and assessed for synergistic killing after 96 h treatment by Bliss Independence (Figure 4H). Here again, SHP2 inhibition markedly enhanced the killing effects of osimertinib in OR1-8 cells, showing an increased excess over Bliss across the matrix of drug combinations (Figure 4H). These data suggest that inhibiting proximal RTK signaling has the potential to overcome RTK-driven osimertinib resistance in *EGFR*-mutated cancers and demonstrates a therapeutic role for inhibitors of proximal RTK signaling, including SHP2 inhibitors, in tumors with reported heterogeneous RTK upregulation in response to prior therapy (Figure 4I). We further assessed the abundance phosphorylated ERK as a surrogate of RAF/MEK/ERK activity SHP2i in parental H1975 cells and four osimertinib-resistant populations (OR2, 3, 5, 6) under both basal (cycling) conditions and after treatment with osimertinib ± RMC-4550 for 24 h. Basal pERK was elevated in all four populations, indicative of elevated RAS effector signaling as a bypass mechanism driving osimertinib resistance. In parental H1975 cells, treatment with 300 or 1000 nM osimertinib (alone) was

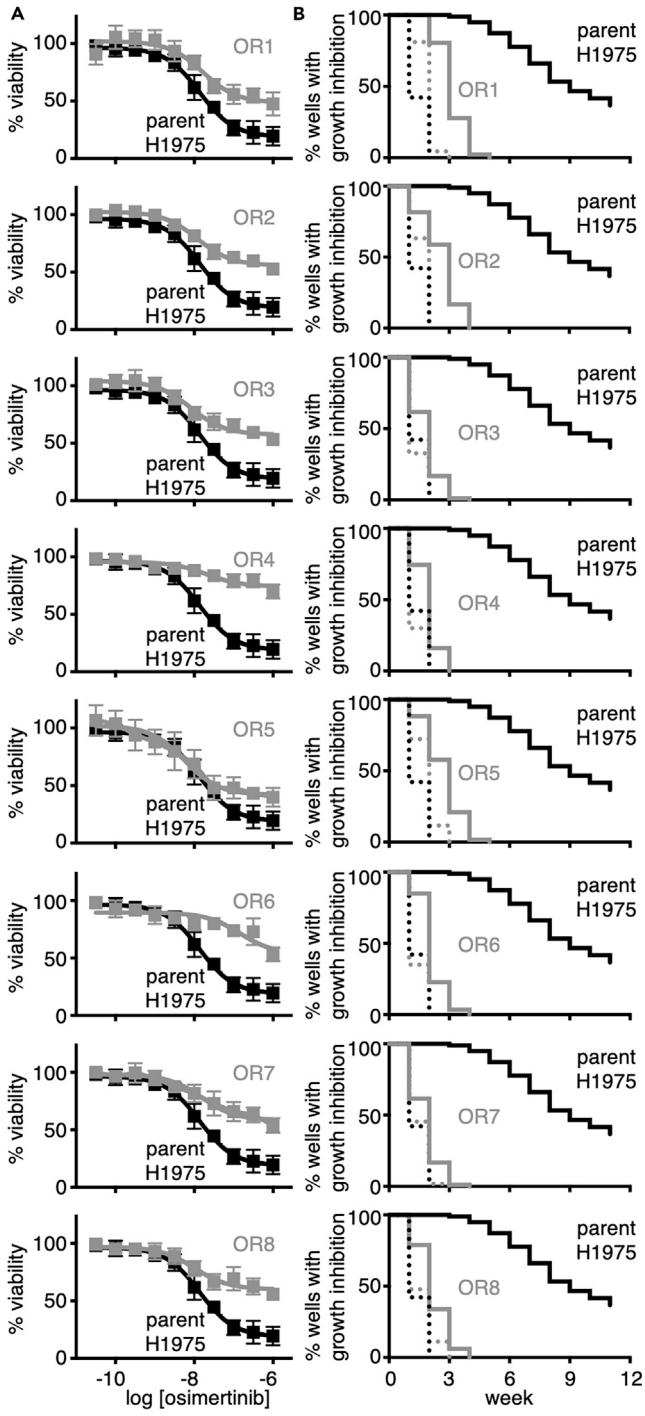

Figure 3. Isolated osimertinib-resistant clones maintain osimertinib resistance upon continued culture

(A) Dose-response curves for osimertinib in parental H1975 cells (black) and osimertinib-resistant H1975 populations (gray) isolated from osimertinib resistance assays. Data in (A) are mean ± SD from n = 3 independent experiments.

(B) H1975 parental (black) or osimertinib-resistant populations (gray) were plated at low density (250 cells/well) in replicate 96-well plates; each plate was either left untreated (dashed line) or treated with 150 nM osimertinib (solid line). Wells were fed and assessed weekly for outgrowth; wells that were >50% confluent were scored as osimertinib resistant. Data are plotted as a Kaplan-Meyer survival curve. Data in (B) are combined from n = 3 independent trials.

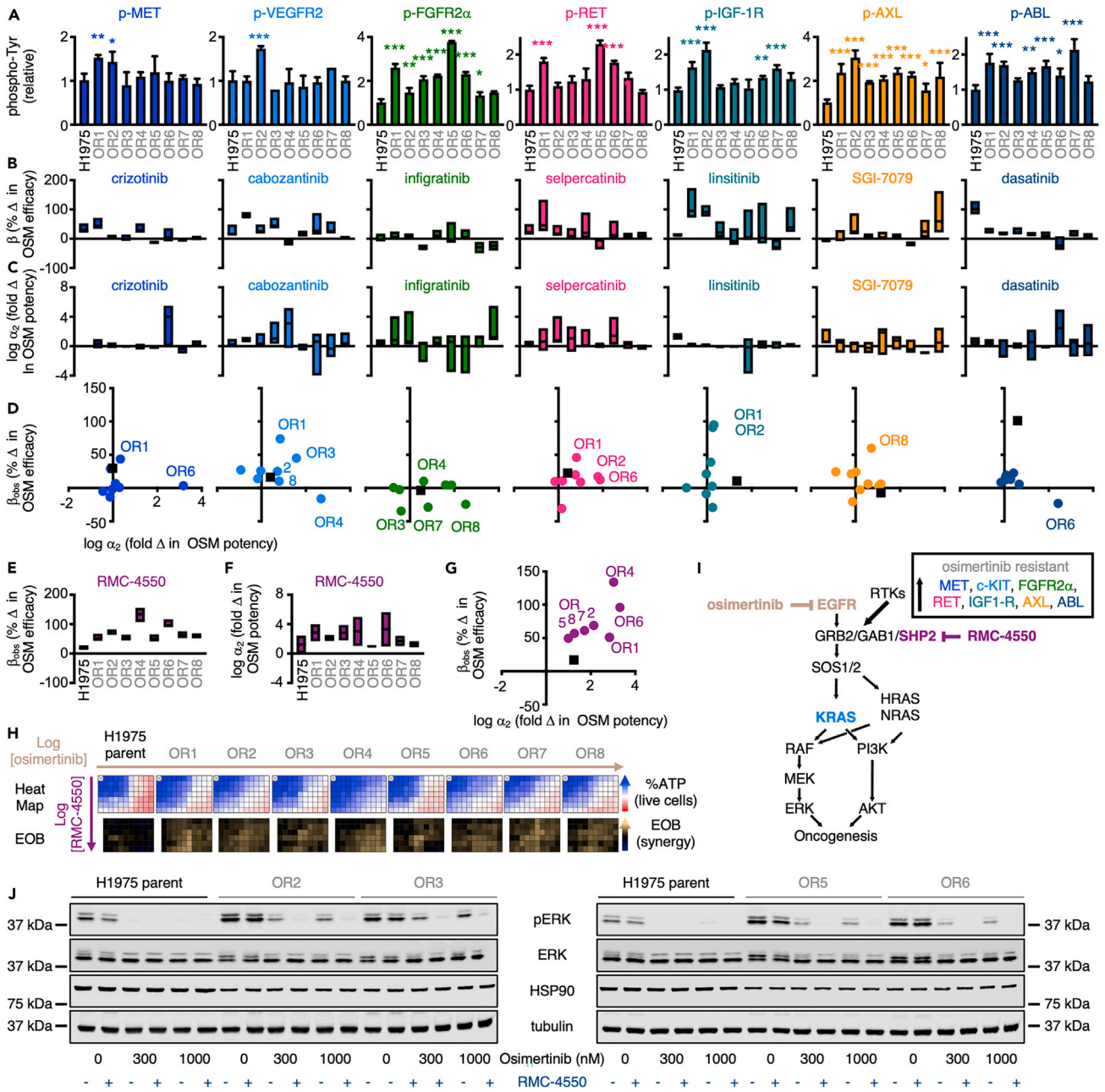

Figure 4. Osimertinib-resistant populations show hyperactivation of multiple RTKs and are sensitive to SHP2 inhibition

(A) Quantitation of tyrosine phosphorylation of the indicated RTKs in whole-cell lysates from osimertinib-resistant H1975 populations OR1-8 relative to parental controls; samples were assessed for RTK phosphorylation using a human RTK phosphorylation antibody array (RayBiotech, complete array data in Figure S2). Data are mean ± SD from n = 3 replicate wells of the RTK array. *p < 0.05; **p < 0.01; ***p < 0.001 vs. parental H1975 cells.

(B–D) Quantitation of the change in % osimertinib efficacy (B, β_{obs}), fold change in osimertinib potency (C, log α_2), and a plot showing the change in osimertinib potency (log α_2) versus efficacy (β_{obs}) (D) from dose-response experiments assessing combined treatment of parental H1975 cells or OR1-8 populations with osimertinib +/− the indicated second RTK or RTK/RAS pathway inhibitor from Figure S4. For (D), cells in the upper right quadrant (positive log α_2 and positive β_{obs}) represent the most promising osimertinib combination for a given cell population. Data in (B) and (C) are shown as the mean and 95% confidence interval, and data in (D) are the mean from n = 3 independent experiments.

(E–G) Quantitation of the change in % osimertinib efficacy (E, β_{obs}), fold change in osimertinib potency (F, log α_2), and a plot showing the change in osimertinib potency (log α_2) versus efficacy (β_{obs}) (G) from dose-response experiments assessing combined treatment of parental H1975 cells or OR1-8 populations with osimertinib +/− the SHP2 inhibitor RMC-4550. Data in E and F are shown as the mean and 95% confidence interval, and data in G are the mean from n = 3 independent experiments.

Figure 4. *Continued*

(H) Parental and osimertinib-resistant H1975 populations were treated with a matrix of doses of osimertinib +/− the SHP2 inhibitor RMC-4550 for four days, and cell viability was assessed using CellTitre glo. Excess over Bliss was calculated for each dose combination as a measure of synergy. Data are the mean from n = 3 independent experiments.

(I) Schematic showing hyperactivation of multiple RTKs driving acquired osimertinib resistance. Inhibition of proximal RTK signaling using a SHP2 inhibitor, but not individual RTK inhibitors, synergizes with osimertinib by enhancing osimertinib efficacy and potency.

(J) Western blots for pERK, ERK, HSP90, and tubulin from whole-cell lysates of parental and osimertinib-resistant H1975 populations (OR2, OR3, OR5, and OR6) left untreated or treated with 300 nM or 1000 nM osimertinib ±300 nM RMC-4550. Western blots are representative of n = 2 independent experiments.

sufficient to inhibit RAF/MEK/ERK signaling (Figure 4J). In contrast, in all four osimertinib-resistant cell lines (OR2, OR3, OR5, and OR6), combined osimertinib + RMC-4550 was needed to fully inhibit ERK phosphorylation (Figure 4J).

Modeling resistance to KRAS^{G12C} inhibitors, trametinib, and tipifarnib

Oncogenic driver mutations in the RTK/RAS/RAF pathway occur in 75%–90% of LUAD. Similar to *EGFR*-mutated LUADs treated with osimertinib, acquired resistance to targeted therapies limits the overall window of their effectiveness to treat patients with LUAD. We sought to determine the extent to which ISRAs could be used as a general model of acquired resistance to agents targeting the RTK/RAS pathway. We therefore sought to model acquired resistance to the covalent KRAS^{G12C} inhibitors adagrasib (Figure 5A) and sotorasib (Figure 5B) in *KRAS*^{G12C}-mutated (H358, H1373) LUAD cells, the MEK inhibitor trametinib in both *KRAS*^{G12V}-mutated (H727) and *NF1*-LOF (H1838) LUAD cells (Figure 5C), and the farnesyltransferase inhibitor (FTI) tipifarnib in *HRAS*^{Q61L}-mutated (H1915) LUAD cells and *HRAS*^{Q61L}-mutated (SMS-CTR) rhabdomyosarcoma cells (Figure 5D). Only a subset of *KRAS*-mutated cell lines show KRAS dependence in 2D adherent culture,[39–43] whereas these same cell lines require KRAS for anchorage-independent growth,[44–50] and some *KRAS*^{G12C}-mutated cells respond well to KRAS^{G12C} inhibitors both *in vivo* and in 3D culture but not 2D adherent culture.[48] Thus, we first established the doses of each inhibitor that inhibits survival ($\geq EC_{50}$) under both 2D (adherent) and 3D (spheroid) conditions in the panel of RTK/RAS-pathway-mutated cell lines by treating cells with increasing doses of the indicated inhibitor and assessing cell viability four days after treatment (Figure S5; EC_{50}–EC_{90} values for each drug/cell line combination are shown in Figures 5E and S5C). ISRAs were then performed using both 2D and 3D inhibitory doses (~EC_{50}–EC_{85}) for each inhibitor/cell line combination (Figures 5A–5D and data not shown). For *KRAS*-mutated or *NF1*-LOF cells treated with either a KRAS^{G12C} inhibitor or trametinib, 3D dose-response curves were the best indicator of doses that should be used in ISRAs; lower doses of adagrasib, sotorasib, or trametinib corresponding to the 3D EC_{50}-EC_{75} caused a 1- to 3-week delay in the outgrowth of cells, whereas cells treated with $\geq EC_{80}$ of inhibitor showed prolonged growth arrest before regaining proliferative capacity (Figures 5A–5C), indicating that these wells had become resistant to the indicated therapeutic. In contrast, treatment of cells with the $\geq EC_{80}$ dose indicated from 2D (adherent) dose-response experiments was lethal to the cultures. We speculate that this is either because the low-density cell seeding for ISRAs does not allow for paracrine signaling and/or because of the inherent differences between performing dose-response experiments over four days versus 6–12 weeks. For HRAS-mutated cells treated with tipifarnib, lower doses corresponding to the 2D EC_{50}-EC_{75} caused a 1- to 3-week delay in the outgrowth of cells, whereas cells treated with $\geq EC_{80}$ showed prolonged growth arrest before regaining proliferative capacity (Figures 5A–5D), indicating that these wells had become tipifarnib resistant. These data show that, in addition to modeling osimertinib, ISRAs can be used to model acquired resistance to multiple therapies targeting the RTK/RAS/ERK pathway.

DISCUSSION

Oncogene-targeted therapies have revolutionized cancer treatment. However, in many cases, single-agent targeting of mutated oncogenes shows less than optimal results, as both intrinsic and acquired resistance can limit the overall effectiveness of these agent. Efforts to identify secondary therapies have focused on either identifying synthetic lethal targets to enhance therapeutic efficacy and overcome intrinsic resistance or identifying and treating acquired resistance after it occurs. In contrast, studies that assess the extent to which drug combinations can delay the onset of acquired resistance and thereby prolong the initial treatment window are often lacking due to the unavailability of cell culture methods to assess acquired resistance. Here, we describe an *in situ* resistance assay, performed in a 96-well culture format, that allows both for the modeling of acquired resistance in large cohorts of independent cultures (180 cultures/condition) and parallel isolation of therapy-resistant populations without the need for ring cloning/colony isolation from large-dish cultures of drug-treated cells. The utility of both a high-throughput method of assessing acquired resistance and the benefit of isolating resistant cultures without the need for additional experimentation makes this a versatile assay in cancer biology.

As a model for assay development, we used osimertinib resistance in *EGFR*-mutated LUAD. Osimertinib is well established as first-line therapy for patients with EGFR-mutated LUAD,[2,3] the mechanisms driving acquired resistance are well defined,[4–13] and mechanism-based treatment of acquired resistance is largely unsuccessful as most patients develop tumors harboring multiple parallel resistance mechanisms simultaneously.[14] We found that osimertinib resistance could be reliably modeled in *EGFR*-mutated LUAD cell lines using doses of osimertinib defined by the individual cell line's dose-response curves. Further, osimertinib-resistance populations could be isolated from resistance assays that showed RTK-dependent resistance mechanisms similar to patient populations, but targeting these resistance mechanisms with RTK inhibitors did not reliably resensitize cells to osimertinib. In contrast, pan-RTK inhibition using an inhibitor of the proximal RTK signaling intermediate SHP2 synergistically enhanced the efficacy and potency of osimertinib across osimertinib-resistant populations. However, even

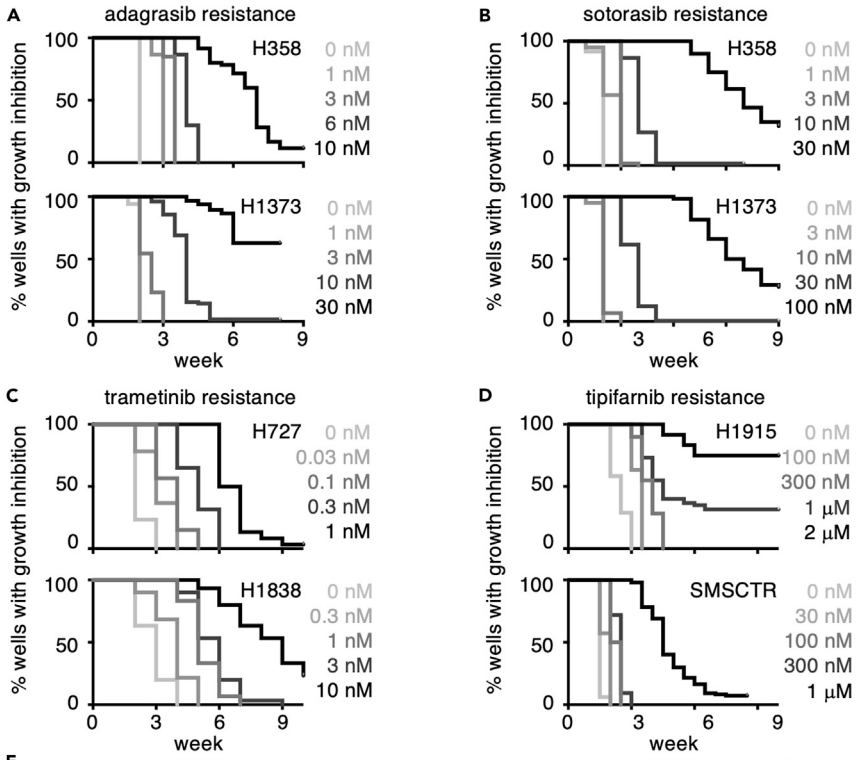

E

	adagrasib (3D)		sotorasib (3D)		trametinib (3D)		tipifarnib (2D)	
	H358	H1373	H358	H1373	H727	H1838	H1915	SMS
EC_{50}	4	12	8	25	0.2	0.5	45	108
EC_{60}	5	16	12	33	0.3	1	85	161
EC_{70}	7	21	18	45	0.4	3	169	250
EC_{75}	8	25	23	54	0.6	5	249	321
EC_{80}	**10**	**31**	**31**	**66**	**0.8**	**9**	**388**	**428**
EC_{85}	**12**	**39**	**44**	**85**	**1.1**	**20**	**666**	**605**
EC_{90}	**16**	**53**	**70**	**118**	**1.8**	**51**	**1362**	**959**

Figure 5. The *in situ* resistance assay can be used to model resistance to RTK/RAS-pathway-targeted therapies

(A–D) *KRAS*^{G12C}-mutated H358 and H1373 cells (A and B), *KRAS*^{G12C}-mutated H727 and NF1-LOF H1838 cells (C), or HRAS-mutated H1915 and SMSCTR cells were plated at low density (250 cells/well) in replicate 96-well plates, and each plate was either left untreated or treated with the indicated dose of sotorasib (A), adagrasib (B), trametinib (C), or tipifarnib (D). Wells were fed and assessed weekly for outgrowth; wells that were >50% confluent were scored as resistant to the given dose of osimertinib-resistant. Data are plotted as a Kaplan-Meyer survival curve and are combined from n = 3 independent trials. Plates treated with ≥ the EC_{80} dose of a given targeted inhibitor (see bold values in E) showed an extended inhibition of growth followed by outgrowth of individual colonies consistent with true drug resistance.

(E) EC_{50}–EC_{90} values from dose-response curves assessing sotorasib (H358, H1373), adagrasib (H358, H1373), trametinib (H727, H1838), or tipifarnib (H1915, SMSCTR) sensitivity. Sotorasib, adagrasib, and trametinib sensitivities were assessed in 3D cultured spheroids; tipifarnib sensitivity was assessed in 2D adherent culture.

though SHP2 inhibition synergized with osimertinib to kill resistant populations, combined EGFR/SHP2 inhibition produced only ~70% killing, highlighting the need for combinations that block the development of resistance rather than treating resistant tumors.

A majority of osimertinib resistance is driven by RTK reactivation, thus, pan-RTK inhibition has the potential to circumvent the development of most forms of osimertinib resistance. Indeed, we show that SHP2 inhibition both delayed the onset of osimertinib resistance and limited the overall percentage of populations able to become osimertinib resistant. Downstream of RTKs, the SHP2 phosphatase acts as an adaptor to recruit the RASGEFs SOS1 and SOS2 to receptor complexes and promote RAS activation. SOS1 inhibition limits both intrinsic and acquired resistance to KRAS^{G12C} inhibitors,[51] suggesting that proximal RTK inhibition may be a general strategy to overcome resistance to targeted therapies in lung adenocarcinoma.[52]

Finally, we show our approach to assessing osimertinib resistance *in situ* can be easily adopted to multiple additional RTK/RAS pathway inhibitors with similar objectively defined drug-dosing parameters. Although studies that identify synergistic drug targets to boost

therapeutic efficacy to RTK/RAS pathway inhibitors abound, there has been a paucity of assays to systematically assess the extent to which these same combinations can limit acquired resistance. We propose that *in situ* resistance assays, performed over a 6- to 12-week period, fill this gap in our arsenal of studies assessing combination therapies for cancer treatment. Further, the ease of testing multiple combinations simultaneously, combined with the recent decision by the FDA to no longer require animal testing for approval of new drugs,[53] make *in situ* resistance assays a cost-effective approach when evaluating therapeutic combinations.

Limitations of the study

The assay presented earlier is conducted in adherent culture conditions for ease of exchanging media during the 1- to 12-week period of the study. We acknowledge that the current approach to scoring each well of each condition is an objective method of scoring. Osimertinib-resistant cell populations cultured from ISRAs are not selected clonally and may represent more than one resistance mechanism within a population. Regarding the aforementioned points, we are currently working toward adapting the assay to spheroid culture and optimizing methods of quantitative scoring and imaging of wells as they reach confluency.

STAR★METHODS

Detailed methods are provided in the online version of this paper and include the following:

- KEY RESOURCES TABLE
- RESOURCE AVAILABILITY
  - Lead contact
  - Materials availability
  - Data and code availability
- EXPERIMENTAL MODEL AND STUDY PARTICIPANT DETAILS
  - Cell culture
- METHOD DETAILS
  - Single dose-response studies
  - Assessment of synergy
  - In situ resistance assays (ISRAs)
  - Preparation of cell lysates and western blot analysis
  - Phosphotyrosine array
- QUANTIFICATION AND STATISTICAL ANALYSIS
- ADDITIONAL RESOURCES

SUPPLEMENTAL INFORMATION

Supplemental information can be found online at https://doi.org/10.1016/j.isci.2023.108711.

ACKNOWLEDGMENTS

This work was supported by funding from the NIH (R01 CA255232 and R21 CA267515 to RLK) and the CDMRP Lung Cancer Research Program (LC180213 to RLK). The funders had no role in the study design, data collection and interpretation, or the decision to submit the work for publication. We thank Dr. Edward Stites (Yale School of Medicine) for helpful discussions during the manuscript's preparation. The opinions and assertions expressed herein are those of the authors and are not to be construed as reflecting the views of Uniformed Services University of the Health Sciences or the United States Department of Defense. Materials are available upon request from RLK.

AUTHOR CONTRIBUTIONS

N.E.S., P.L.T., and R.L.K. designed the experiments and analyzed the data; N.E.S., P.L.T., and R.L.K. performed most of the experiments; A.J.L. and B.R.D. performed resistance assays; J.E.H. assisted with dose-response curves; N.E.S. and R.L.K. wrote the manuscript; B.R.D. edited the manuscript.

DECLARATION OF INTERESTS

The authors declare no competing interests.

Received: July 13, 2023
Revised: October 31, 2023
Accepted: December 8, 2023
Published: December 11, 2023

REFERENCES

1. Gridelli, C., Rossi, A., Carbone, D.P., Guarize, J., Karachaliou, N., Mok, T., Petrella, F., Spaggiari, L., and Rosell, R. (2015). Non-small-cell lung cancer. Nat. Rev. Dis. Prim. *1*, 15009.
2. Soria, J.C., Ohe, Y., Vansteenkiste, J., Reungwetwattana, T., Chewaskulyong, B., Lee, K.H., Dechaphunkul, A., Imamura, F., Nogami, N., Kurata, T., et al. (2018). Osimertinib in Untreated EGFR-Mutated Advanced Non-Small-Cell Lung Cancer. N. Engl. J. Med. *378*, 113–125.
3. Ramalingam, S.S., Vansteenkiste, J., Planchard, D., Cho, B.C., Gray, J.E., Ohe, Y., Zhou, C., Reungwetwattana, T., Cheng, Y., Chewaskulyong, B., et al. (2020). Overall Survival with Osimertinib in Untreated, EGFR-Mutated Advanced NSCLC. N. Engl. J. Med. *382*, 41–50.
4. Eberlein, C.A., Stetson, D., Markovets, A.A., Al-Kadhimi, K.J., Lai, Z., Fisher, P.R., Meador, C.B., Spitzler, P., Ichihara, E., Ross, S.J., et al. (2015). Acquired Resistance to the Mutant-Selective EGFR Inhibitor AZD9291 Is Associated with Increased Dependence on RAS Signaling in Preclinical Models. Cancer Res. *75*, 2489–2500.
5. Shi, P., Oh, Y.T., Zhang, G., Yao, W., Yue, P., Li, Y., Kanteti, R., Riehm, J., Salgia, R., Owonikoko, T.K., et al. (2016). Met gene amplification and protein hyperactivation is a mechanism of resistance to both first and third generation EGFR inhibitors in lung cancer treatment. Cancer Lett. *380*, 494–504.
6. La Monica, S., Cretella, D., Bonelli, M., Fumarola, C., Cavazzoni, A., Digiacomo, G., Flammini, L., Barocelli, E., Minari, R., Naldi, N., et al. (2017). Trastuzumab emtansine delays and overcomes resistance to the third-generation EGFR-TKI osimertinib in NSCLC EGFR mutated cell lines. J. Exp. Clin. Cancer Res. *36*, 174.
7. Mancini, M., Gal, H., Gaborit, N., Mazzeo, L., Romaniello, D., Salame, T.M., Lindzen, M., Mahlknecht, G., Enuka, Y., Burton, D.G., et al. (2018). An oligoclonal antibody durably overcomes resistance of lung cancer to third-generation EGFR inhibitors. EMBO Mol. Med. *10*, 294–308.
8. Romaniello, D., Mazzeo, L., Mancini, M., Marrocco, I., Noronha, A., Kreitman, M., Srivastava, S., Ghosh, S., Lindzen, M., Salame, T.M., et al. (2018). A Combination of Approved Antibodies Overcomes Resistance of Lung Cancer to Osimertinib by Blocking Bypass Pathways. Clin. Cancer Res. *24*, 5610–5621.
9. Park, J.H., Choi, Y.J., Kim, S.Y., Lee, J.E., Sung, K.J., Park, S., Kim, W.S., Song, J.S., Choi, C.M., Sung, Y.H., et al. (2016). Activation of the IGF1R pathway potentially mediates acquired resistance to mutant-selective 3rd-generation EGF receptor tyrosine kinase inhibitors in advanced non-small cell lung cancer. Oncotarget *7*, 22005–22015.
10. Kim, D., Bach, D.H., Fan, Y.H., Luu, T.T.T., Hong, J.Y., Park, H.J., and Lee, S.K. (2019). AXL degradation in combination with EGFR-TKI can delay and overcome acquired resistance in human non-small cell lung cancer cells. Cell Death Dis. *10*, 361.
11. Taniguchi, H., Yamada, T., Wang, R., Tanimura, K., Adachi, Y., Nishiyama, A., Tanimoto, A., Takeuchi, S., Araujo, L.H., Boroni, M., et al. (2019). AXL confers intrinsic resistance to osimertinib and advances the emergence of tolerant cells. Nat. Commun. *10*, 259.
12. Jimbo, T., Hatanaka, M., Komatsu, T., Taira, T., Kumazawa, K., Maeda, N., Suzuki, T., Ota, M., Haginoya, N., Isoyama, T., and Fujiwara, K. (2019). DS-1205b, a novel selective inhibitor of AXL kinase, blocks resistance to EGFR-tyrosine kinase inhibitors in a non-small cell lung cancer xenograft model. Oncotarget *10*, 5152–5167.
13. Namba, K., Shien, K., Takahashi, Y., Torigoe, H., Sato, H., Yoshioka, T., Takeda, T., Kurihara, E., Ogoshi, Y., Yamamoto, H., et al. (2019). Activation of AXL as a Preclinical Acquired Resistance Mechanism Against Osimertinib Treatment in EGFR-Mutant Non-Small Cell Lung Cancer Cells. Mol. Cancer Res. *17*, 499–507.
14. Roper, N., Brown, A.L., Wei, J.S., Pack, S., Trindade, C., Kim, C., Restifo, O., Gao, S., Sindiri, S., Mehrabadi, F., et al. (2020). Clonal Evolution and Heterogeneity of Osimertinib Acquired Resistance Mechanisms in EGFR Mutant Lung Cancer. Cell Rep. Med. *1*, 100007.
15. Cunnick, J.M., Dorsey, J.F., Munoz-Antonia, T., Mei, L., and Wu, J. (2000). Requirement of SHP2 binding to Grb2-associated binder-1 for mitogen-activated protein kinase activation in response to lysophosphatidic acid and epidermal growth factor. J. Biol. Chem. *275*, 13842–13848.
16. Kiyatkin, A., Aksamitiene, E., Markevich, N.I., Borisov, N.M., Hoek, J.B., and Kholodenko, B.N. (2006). Scaffolding protein Grb2-associated binder 1 sustains epidermal growth factor-induced mitogenic and survival signaling by multiple positive feedback loops. J. Biol. Chem. *281*, 19925–19938.
17. Sodir, N.M., Pathria, G., Adamkewicz, J.I., Kelley, E.H., Sudhamsu, J., Merchant, M., Chiarle, R., and Maddalo, D. (2023). SHP2: A Pleiotropic Target at the Interface of Cancer and Its Microenvironment. Cancer Discov. Of1–Of17.
18. Plana, D., Palmer, A.C., and Sorger, P.K. (2022). Independent Drug Action in Combination Therapy: Implications for Precision Oncology. Cancer Discov. *12*, 606–624.
19. Pritchard, J.R., Lauffenburger, D.A., and Hemann, M.T. (2012). Understanding resistance to combination chemotherapy. Drug Resist. Updates *15*, 249–257.
20. Bozic, I., Reiter, J.G., Allen, B., Antal, T., Chatterjee, K., Shah, P., Moon, Y.S., Yaqubie, A., Kelly, N., Le, D.T., et al. (2013). Evolutionary dynamics of cancer in response to targeted combination therapy. Elife *2*, e00747.
21. Tanaka, N., Lin, J.J., Li, C., Ryan, M.B., Zhang, J., Kiedrowski, L.A., Michel, A.G., Syed, M.U., Fella, K.A., Sakhi, M., et al. (2021). Clinical Acquired Resistance to KRAS(G12C) Inhibition through a Novel KRAS Switch-II Pocket Mutation and Polyclonal Alterations Converging on RAS-MAPK Reactivation. Cancer Discov. *11*, 1913–1922.
22. Fu, K., Xie, F., Wang, F., and Fu, L. (2022). Therapeutic strategies for EGFR-mutated non-small cell lung cancer patients with osimertinib resistance. J. Hematol. Oncol. *15*, 173.
23. Oxnard, G.R., Hu, Y., Mileham, K.F., Husain, H., Costa, D.B., Tracy, P., Feeney, N., Sholl, L.M., Dahlberg, S.E., Redig, A.J., et al. (2018). Assessment of Resistance Mechanisms and Clinical Implications in Patients With EGFR T790M-Positive Lung Cancer and Acquired Resistance to Osimertinib. JAMA Oncol. *4*, 1527–1534.
24. Bernards, R. (2014). Finding effective cancer therapies through loss of function genetic screens. Curr. Opin. Genet. Dev. *24*, 23–29.
25. Shalem, O., Sanjana, N.E., Hartenian, E., Shi, X., Scott, D.A., Mikkelson, T., Heckl, D., Ebert, B.L., Root, D.E., Doench, J.G., and Zhang, F. (2014). Genome-scale CRISPR-Cas9 knockout screening in human cells. Science *343*, 84–87.
26. Anderson, G.R., Winter, P.S., Lin, K.H., Nussbaum, D.P., Cakir, M., Stein, E.M., Soderquist, R.S., Crawford, L., Leeds, J.C., Newcomb, R., et al. (2017). A Landscape of Therapeutic Cooperativity in KRAS Mutant Cancers Reveals Principles for Controlling Tumor Evolution. Cell Rep. *20*, 999–1015.
27. Ohara, S., Suda, K., and Mitsudomi, T. (2021). Cell Line Models for Acquired Resistance to First-Line Osimertinib in Lung Cancers-Applications and Limitations. Cells *10*.
28. Tang, Z.H., Su, M.X., Guo, X., Jiang, X.M., Jia, L., Chen, X., and Lu, J.J. (2018). Increased Expression of IRE1alpha Associates with the Resistant Mechanism of Osimertinib (AZD9291)-resistant non-small Cell Lung Cancer HCC827/OSIR Cells. Anti Cancer Agents Med. Chem. *18*, 550–555.
29. Tang, Z.H., Jiang, X.M., Guo, X., Fong, C.M.V., Chen, X., and Lu, J.J. (2016). Characterization of osimertinib (AZD9291)-resistant non-small cell lung cancer NCI-H1975/OSIR cell line. Oncotarget *7*, 81598–81610.
30. Codony-Servat, J., Viteri, S., Codony-Servat, C., Ito, M., Bracht, J.W.P., Berenguer, J., Chaib, I., Molina-Vila, M.A., Karachaliou, N., and Rosell, R. (2019). Hsp90 inhibitors enhance the antitumoral effect of osimertinib in parental and osimertinib-resistant non-small cell lung cancer cell lines. Transl. Lung Cancer Res. *8*, 340–351.
31. Fukuda, K., Takeuchi, S., Arai, S., Kita, K., Tanimoto, A., Nishiyama, A., and Yano, S. (2020). Glycogen synthase kinase-3 inhibition overcomes epithelial-mesenchymal transition-associated resistance to osimertinib in EGFR-mutant lung cancer. Cancer Sci. *111*, 2374–2384.
32. Murakami, Y., Kusakabe, D., Watari, K., Kawahara, A., Azuma, K., Akiba, J., Taniguchi, M., Kuwano, M., and Ono, M. (2022). AXL/CDCP1/SRC axis confers acquired resistance to osimertinib in lung cancer. Sci. Rep. *12*, 8983.
33. Kurppa, K.J., Liu, Y., To, C., Zhang, T., Fan, M., Vajdi, A., Knelson, E.H., Xie, Y., Lim, K., Cejas, P., et al. (2020). Treatment-Induced Tumor Dormancy through YAP-Mediated Transcriptional Reprogramming of the Apoptotic Pathway. Cancer Cell *37*, 104–122.e12.
34. Tricker, E.M., Xu, C., Uddin, S., Capelletti, M., Ercan, D., Ogino, A., Pratilas, C.A., Rosen, N., Gray, N.S., Wong, K.K., and Jänne, P.A. (2015). Combined EGFR/MEK Inhibition Prevents the Emergence of Resistance in EGFR-Mutant Lung Cancer. Cancer Discov. *5*, 960–971.
35. Nichols, R.J., Haderk, F., Stahlhut, C., Schulze, C.J., Hemmati, G., Wildes, D., Tzitzilonis, C., Mordec, K., Marquez, A., Romero, J., et al. (2018). RAS nucleotide cycling underlies the SHP2 phosphatase dependence of mutant

BRAF-NF1- and RAS-driven cancers. Nat. Cell Biol. *20*, 1064–1073.

36. de Bruin, E.C., Cowell, C., Warne, P.H., Jiang, M., Saunders, R.E., Melnick, M.A., Gettinger, S., Walther, Z., Wurtz, A., Heynen, G.J., et al. (2014). Reduced NF1 expression confers resistance to EGFR inhibition in lung cancer. Cancer Discov. *4*, 606–619.
37. Meyer, C.T., Wooten, D.J., Paudel, B.B., Bauer, J., Hardeman, K.N., Westover, D., Lovly, C.M., Harris, L.A., Tyson, D.R., and Quaranta, V. (2019). Quantifying Drug Combination Synergy along Potency and Efficacy Axes. Cell Syst. *8*, 97–108.e16.
38. Wooten, D.J., Meyer, C.T., Lubbock, A.L.R., Quaranta, V., and Lopez, C.F. (2021). MuSyC is a consensus framework that unifies multi-drug synergy metrics for combinatorial drug discovery. Nat. Commun. *12*, 4607.
39. Balbin, O.A., Prensner, J.R., Sahu, A., Yocum, A., Shankar, S., Malik, R., Fermin, D., Dhanasekaran, S.M., Chandler, B., Thomas, D., et al. (2013). Reconstructing targetable pathways in lung cancer by integrating diverse omics data. Nat. Commun. *4*, 2617.
40. Singh, A., Sweeney, M.F., Yu, M., Burger, A., Greninger, P., Benes, C., Haber, D.A., and Settleman, J. (2012). TAK1 inhibition promotes apoptosis in KRAS-dependent colon cancers. Cell *148*, 639–650.
41. Scholl, C., Fröhling, S., Dunn, I.F., Schinzel, A.C., Barbie, D.A., Kim, S.Y., Silver, S.J., Tamayo, P., Wadlow, R.C., Ramaswamy, S., et al. (2009). Synthetic lethal interaction between oncogenic KRAS dependency and STK33 suppression in human cancer cells. Cell *137*, 821–834.
42. Lamba, S., Russo, M., Sun, C., Lazzari, L., Cancelliere, C., Grernrum, W., Lieftink, C., Bernards, R., Di Nicolantonio, F., and Bardelli, A. (2014). RAF suppression synergizes with MEK inhibition in KRAS mutant cancer cells. Cell Rep. *8*, 1475–1483.
43. Singh, A., Greninger, P., Rhodes, D., Koopman, L., Violette, S., Bardeesy, N., and Settleman, J. (2009). A gene expression signature associated with "K-Ras addiction" reveals regulators of EMT and tumor cell survival. Cancer Cell *15*, 489–500.
44. Fujita-Sato, S., Galeas, J., Truitt, M., Pitt, C., Urisman, A., Bandyopadhyay, S., Ruggero, D., and McCormick, F. (2015). Enhanced MET Translation and Signaling Sustains K-Ras-Driven Proliferation under Anchorage-Independent Growth Conditions. Cancer Res. *75*, 2851–2862.
45. Rotem, A., Janzer, A., Izar, B., Ji, Z., Doench, J.G., Garraway, L.A., and Struhl, K. (2015). Alternative to the soft-agar assay that permits high-throughput drug and genetic screens for cellular transformation. Proc. Natl. Acad. Sci. USA *112*, 5708–5713.
46. Zhang, Z., Jiang, G., Yang, F., and Wang, J. (2006). Knockdown of mutant K-ras expression by adenovirus-mediated siRNA inhibits the *in vitro* and *in vivo* growth of lung cancer cells. Cancer Biol. Ther. *5*, 1481–1486.
47. McCormick, F. (2015). KRAS as a Therapeutic Target. Clin. Cancer Res. *21*, 1797–1801.
48. Janes, M.R., Zhang, J., Li, L.S., Hansen, R., Peters, U., Guo, X., Chen, Y., Babbar, A., Firdaus, S.J., Darjania, L., et al. (2018). Targeting KRAS Mutant Cancers with a Covalent G12C-Specific Inhibitor. Cell *172*, 578–589.e17.
49. Sheffels, E., Sealover, N.E., Wang, C., Kim, D.H., Vazirani, I.A., Lee, E., M Terrell, E., Morrison, D.K., Luo, J., and Kortum, R.L. (2018). Oncogenic RAS isoforms show a hierarchical requirement for the guanine nucleotide exchange factor SOS2 to mediate cell transformation. Sci. Signal. *11*, eaar8371.
50. Sheffels, E., Sealover, N.E., Theard, P.L., and Kortum, R.L. (2021). Anchorage-independent growth conditions reveal a differential SOS2 dependence for transformation and survival in RAS-mutant cancer cells. Small GTPases *12*, 67–78.
51. Thatikonda, V., Lu, H., Jurado, S., Kostyrko, K., Bristow, C.A., Bosch, K., Feng, N., Gao, S., Gerlach, D., Gmachl, M., et al. (2023). Combined KRASG12C and SOS1 inhibition enhances and extends the anti-tumor response in KRASG12C-driven cancers by addressing intrinsic and acquired resistance. Preprint at bioRxiv. https://doi.org/10.1101/2023.01.23.525210.
52. Sheffels, E., and Kortum, R.L. (2021). Breaking Oncogene Addiction: Getting RTK/RAS-Mutated Cancers off the SOS. J. Med. Chem. *64*, 6566–6568.
53. Wadman, M. (2023). FDA no longer has to require animal testing for new drugs. Science *379*, 127–128.
54. Theard, P.L., Sheffels, E., Sealover, N.E., Linke, A.J., Pratico, D.J., and Kortum, R.L. (2020). Marked synergy by vertical inhibition of EGFR signaling in NSCLC spheroids shows SOS1 is a therapeutic target in EGFR-mutated cancer. Elife *9*, e58204.

STAR★METHODS

KEY RESOURCES TABLE

REAGENT or RESOURCE	SOURCE	IDENTIFIER
Antibodies		
Rabbit monoclonal anti-phospho p44/42 MAPK (Erk1/2) (Thr202/ Tyr204)	Cell Signaling Technology	Cat#4370; RRID: AB_2315112
Mouse monoclonal anti-p44/42 MAPK (Erk1/2)	Cell Signaling Technology	Cat#4696; RRID: AB_390780
Mouse monoclonal anti-HSP90 alpha	Santa Cruz	Cat#sc-515081; RRID: AB_2943315
Rabbit recombinant anti-alpha tubulin	abcam	Cat#ab176560; RRID: AB_2860019
IRDye® 680RD Donkey anti-Rabbit IgG Secondary Antibody	LICOR	Cat#926-68073
IRDye® 800CW Donkey anti-Mouse IgG Secondary Antibody	LICOR	Cat#926-32212
Chemicals, peptides, and recombinant proteins		
osimertinib (AZD9291; 3rd gen EGFR inhibitor)	Selleck Chemicals	S7297; CAS: 1421373-65-0
RMC-4550 (SHP2 inhibitor)	Selleck Chemicals	S8718; CAS: 2172651
SHP099 (SHP2 inhibitor)	Selleck Chemicals	S6388; CAS: 1801747-42-1
crizotinib (c-Met and ROS1 inhibitor)	Selleck Chemicals	S1068; CAS: 877399-52-5
cabozantinib (XL184; VEGFR2 inhibitor)	Selleck Chemicals	S1119; CAS: 849217-68-1
infigratinib (BGJ398; FGFR inhibitor)	Selleck Chemicals	S2183; CAS: 872511-34-7
selpercatinib (LOXO-292; RET inhibitor)	Selleck Chemicals	S8781; CAS: 2152628-33-4
linsitinib (OSI-906; IGF1R inhibitor)	Selleck Chemicals	S1091; CAS: 867160-71-2
SGI-7079 (AXL inhibitor)	Selleck Chemicals	S7847; CAS: 1239875-86-5
dasatinib (SRC/ABL/c-Kit inhibitor)	Selleck Chemicals	S1021; CAS: 302962-49-8
adagrasib (MRTX849; KRASG12C inhibitor)	Selleck Chemicals	S8884; CAS: 2326521-71-3
sotorasib (AMG510; KRASG12C inhibitor)	Selleck Chemicals	S8830; CAS: 2296729-00-3
trametinib (GSK1120212; MEK inhibitor)	Selleck Chemicals	S2673; CAS: 871700-17-3
tipifarnib (farnesyl transferase inhibitor)	Selleck Chemicals	S1453; CAS: 192185-72-1
Protease inhibitor cocktail	Biotool	Cat#B14002
Phosphatase inhibitor cocktail	Biotool	Cat#B15002
Critical commercial assays		
CellTiter-Glo 2.0®	Promega	G9243
Trans-Blot® Turbo Transfer System	BioRad	17001917
Human RTK Phosphorylation Array G1	RayBiotech	AAH-PRTK-G1-8
Experimental models: Cell lines		
NCI-H1975	Obtained from Udayan Guha, available at ATCC	RRID:CVCL_UE30
HCC827	Obtained from Udayan Guha, available at ATCC	RRID:CVCL_DH92
PC9	Obtained from Udayan Guha, available at NCI-DTP or ATCC	RRID:CVCL_B260
PC9-TM	de Bruin et al., 2014	N/A
H358	ATCC	RRID:CVCL_1559
H1373	ATCC	RRID:CVCL_1465

(*Continued on next page*)

Continued

REAGENT or RESOURCE	SOURCE	IDENTIFIER
H727	ATCC	RRID:CVCL_1584
H1838	ATCC	RRID:CVCL_1499
H1915	ATCC	RRID:CVCL_1505
SMS-CTR	Obtained from Marielle Yohe	RRID:CVCL_A770
Software and algorithms		
Prism version 9.2.0	Graphpad	RRID:SCR_002798
ImageStudioLite	Licor	RRID:SCR_013715
Multi-dimensional Synergy of Combinations (MuSyC)	Meyer et al. 2019	N/A
Other		
96-well white-walled tissue culture plates	Perkin Elmer	Cat#6004480
96-well clear-walled tissue culture plates	CELLTREAT	Cat#229195
96-well ultra-low attachment round bottomed plates	Corning	Cat#7007
96-well Nunc Nucleon Sphera microplates	ThermoFisher	Cat#174929
384-well white-walled culture plates	Perkin Elmer	Cat#6007480

RESOURCE AVAILABILITY

Lead contact

Further information and requests for resources and reagents should be directed to and will be fulfilled by the lead contact, Dr. Robert L. Kortum (robert.kortum@usuhs.edu).

Materials availability

Osimertinib-resistant cell lines generated in this study are available via MTA upon request from Dr. Robert L. Kortum (robert.kortum@usuhs.edu).

Data and code availability

- All data reported in this paper will be shared by the lead contact upon request.
- This paper does not report original code.
- Any additional information required to reanalyze the data reported in this paper is available from the lead contact upon request.
- All authors have approved the experiments and all experiments conform to the relevant regulatory standards.

EXPERIMENTAL MODEL AND STUDY PARTICIPANT DETAILS

Cell culture

Cell lines were cultured at 37°C and 5% CO_2. HCC827 (obtained from Udayan Guha; RRID:CVCL_DH92), NCI-H1975 (obtained from Udayan Guha, RRID:CVCL_UE30), PC9 (obtained from Udayan Guha; RRID:CVCL_B260), PC9-TM,[36] H358 (ATCC; RRID:CVCL_1559), H1373 (ATCC; RRID:CVCL_1465), H727 (ATCC; RRID:CVCL_1584), H1838 (ATCC; RRID:CVCL_1499), and H1915 (ATCC; RRID:CVCL_1505) cells were maintained in Roswell Park Memorial Institute medium (RPMI), SMS-CTR cells (obtained from Marielle Yohe; RRID:CVCL_A770) were maintained in Dulbecco's Modified Eagles Medium (DMEM), each supplemented with 10% fetal bovine serum and 1% penicillin-streptomycin. Cell lines were authenticated by STR profiling in the past three years and confirmed as mycoplasma negative. Osimertinib-resistant (OR1-8) H1975 cells were isolated from ISRAs treated with 150 nM osimertinib (S7297, Selleck Chemicals, Houston, TX, USA) for > 6 weeks. OR1-8 populations were maintained under osimertinib selection during expansion.

METHOD DETAILS

Single dose-response studies

For adherent studies, cells were seeded at 500 cells per well in 100 μL in the inner-60 wells of 96-well white-walled culture plates (Perkin Elmer #6004480) and allowed to attach for 24 hours prior to drug treatment. For 3D spheroid studies cells were seeded at 500-1,000 cells per well in 100 μL in the inner-60 wells of 96-well ultra-low attachment round bottomed plates (Corning #7007) or Nunc Nucleon Sphera microplates

(ThermoFisher #174929) and allowed to coalesce as spheroids for 24-48 hours prior to drug treatment. Cells were treated with drug for 96 hours prior to assessment of cell viability using CellTiter-Glo® 2.0 (G9243, Promega, Madison, WI, USA).

Assessment of synergy

Cells were seeded at 200 cells per well in 40 μL in the inner-312 wells of 384-well white-walled culture plates (Perkin Elmer #6007480) and allowed to attach for 24-hours prior to drug treatment. To assess the effectiveness of secondary therapies +/- osimertinib, cells were treated with increasing doses (log^{-10} – log^{-5}; 0.1 nM – 10,000 nM) of crizotinib (S1068, Selleck Chemicals, Houston, TX, USA), cabozantinib (S1119, Selleck Chemicals, Houston, TX, USA), infigratinib (S2183, Selleck Chemicals, Houston, TX, USA), selpercatinib (S8781, Selleck Chemicals, Houston, TX, USA), linsitinib (S1091, Selleck Chemicals, Houston, TX, USA), SGI-7079 (S7847, Selleck Chemicals, Houston, TX, USA), dasatinib (S1021, Selleck Chemicals, Houston, TX, USA), or RMC-4550 (S8718, Selleck Chemicals, Houston, TX, USA) +/- 10 nM osimertinib. To assess the extent to which each secondary inhibitor enhanced the effectiveness of osimertinib, cells were treated with increasing doses (log^{-11} – log^{-6}; 0.01 nM – 1000 nM) of osimertinib +/- 100 nM or 300 nM of one of the above inhibitors. To assess drug-drug synergy across a matrix of dose combinations for the osimertinib/RMC-4550 combination, cells were treated with increasing doses of RMC-4550 alone ($log^{-9.5}$ – log^{-5}; 0.3 nM – 10,000 nM), osimertinib alone ($log^{-10.5}$ – log^{-6}; 0.03 nM – 1000 nM), or osimertinib + RMC-4550 in a 6 × 10 matrix of drug combinations on a semi-log scale. Cells were treated with drug for 96 hours prior to assessment of cell viability using CellTiter-Glo® 2.0 (G9243, Promega, Madison, WI, USA). Values collected from inhibitor treated wells were normalized to values from DMSO control wells.

In situ resistance assays (ISRAs)

Cells were seeded at 250 cells/well in 100 μL in replicate 96-well tissue culture plates (CELLTREAT #229195) and allowed to adhere for 24 hours prior to drug treatment. Plates were then either fed with an additional 100 μL of media or treated with the indicated single dose of targeted inhibitor (osimertinib, sotorasib (Selleck Chemicals; S8830), adagrasib (S8884, Selleck Chemicals, Houston, TX, USA), trametinib (S2673, Selleck Chemicals, Houston, TX, USA), or tipifarnib (S1453, Selleck Chemicals, Houston, TX, USA) corresponding to ~ EC_{50} – EC_{85} dose of that drug. For Figure 3, plates were treated with the indicated drug combinations. The inner 60 wells of each plate were assessed weekly for signs of cell growth using a 4x objective, with wells reaching >50% confluence scored as resistant. Each plate used for ISRAs had the media in each well replaced once a week to refresh media or media diluted with the indicated dose or combination dose of targeted inhibitor(s); media was removed from the entire plate in a cell culture hood by quickly inverting the plate into an autoclave bin lined with paper towels to avoid cross-contamination of wells and wells in each plate were refilled with a multi-channel repeating pipettor.

Preparation of cell lysates and western blot analysis

Cells were lysed in RIPA buffer (1% NP-40, 0.1% SDS, 0.1% Na-deoxycholate, 10% glycerol, 0.137 M NaCl, 20 mM Tris pH [8.0], protease (Biotool #B14002) and phosphatase (Biotool #B15002) inhibitor cocktails) for 20 minutes at 4°C and spun at 10,000 RPM for 10 minutes. Clarified lysates were boiled in SDS sample buffer containing 100 mM DTT for 10 minutes prior to western blotting. Proteins were resolved by sodium dodecyl sulfate-polyacrylamide (Criterion TGX precast) gel electrophoresis and transferred to nitrocellulose membranes using the Trans-Blot® Turbo Transfer System (BioRad, Hercules, CA, USA). The nitrocellulose membrane was incubated overnight at 4°C with either: anti-pERK1/2 (4370, Cell Signaling, Danvers, MA, USA, 1:1,000), anti-ERK1/2 (4696, Cell Signaling, Danvers, MA, USA, 1:1000), anti-HSP90 alpha (sc-515081; Santa Cruz Biotechnology, Dallas, TX, USA, 1:10,000), or anti-alpha tubulin (ab176560, abcam, Cambridge, UK, 1:20,000). Anti-mouse and anti-rabbit secondary antibodies conjugated to IRDye680 (926-68073, LI-COR Biosciences, Lincoln, Nebraska, USA, 1:10,000) or IRDye800 (926-32212, LI-COR Biosciences, Lincoln, Nebraska, USA, 1:10,000) were used to probe primary antibodies. Western blot protein bands were detected using the Odyssey system and ImageStudioLite Software (LI-COR Biosciences, Lincoln, Nebraska, USA).

Phosphotyrosine array

Cells were lysed as described above. Clarified lysates were diluted to 1 mg/mL in RIPA buffer prior to assessing for RTK phosphorylation using a Human RTK Phosphorylation Array G1 (RayBiotech, AAH-PRTK-G1-8) per manufacturer's instructions. Slides were shipped to RayBiotech for data acquisition. For each phosphorylated protein, data were normalized to the average level of phosphorylation observed from two independent isolates of H1975 parental lysate.

QUANTIFICATION AND STATISTICAL ANALYSIS

Dose response data were analyzed by non-linear regression using GraphPad Prism 9.2.0 (Graph Pad, San Diego, CA, USA) from n=3 independent trials. Synergy was first assessed by Bliss Independence analysis and reported as a matrix of excess over Bliss values as previously described[54] from n=3 independent trials. To deconvolute synergistic efficacy vs. potency, we further analyzed drug-drug studies with Multi-dimensional Synergy of Combinations (MuSyC) Analysis[37,38] using an online tool (https://musyc.lolab.xyz). Data were plotted using GraphPad Prism 9.2.0 and are presented as mean +/- 95% confidence interval. Statistical significance is specifically not assigned to MuSyC analysis, as the authors report that the magnitude of each change allows the reader to interpret the data without the assignment of significance. ISRAs were plotted as a Kaplan-Meyer survival curve; significance was assessed by pairwise comparison of Kaplan-Meyer curves using GraphPad

Prism 9.2.0 (Graph Pad, San Diego, CA, USA). ISRA data were pooled from n=3 independent experiments. To analyze data for each phosphorylated protein in the phosphotyrosine array (RayBiotech, AAH-PRTK-G1-8), data were normalized to the average level of phosphorylation observed from two independent isolates of H1975 parental lysate. Statistical significance was assessed by two-way ANOVA followed by a Bonferroni correction to adjust for multiple comparisons using Prism 9.2.0 from n=3 replicate wells of the RTK array. All data analysis methods used to determine significance met the assumptions of the specific statistical approach. In Figure 4A * $p < 0.05$; ** $p<0.01$; *** $p < 0.001$ vs parental H1975 cells.

ADDITIONAL RESOURCES

This work is not part of a clinical trial and there are no clinical registry numbers to disclose.